Fiber laser-based scanning lidar for space rendezvous and docking

Yuan Luo,[1,2] Yan He,[1,*] Min Gao,[1] Cuiyun Zhou,[1] Huaguo Zang,[1] Linjun Lei,[1] Kedi Xie,[1] Yan Yang,[1] Wei Shi,[1] Xia Hou,[1] and Weibiao Chen[1]

[1]Key Laboratory of Space Laser Communication and Detection Technology, Shanghai Institute of Optics and Fine Mechanics, Chinese Academy of Sciences, Shanghai 201800, China

[2]University of Chinese Academy of Sciences, Beijing 100049, China

*Corresponding author: heyan@siom.ac.cn

Received 19 September 2014; revised 19 January 2015; accepted 5 February 2015; posted 9 February 2015 (Doc. ID 223061); published 19 March 2015

Lidar systems have played an important role in space rendezvous and docking (RVD). A new type of scanning lidar is developed using a high-repetition-rate pulsed fiber laser and a position detector. It will be a candidate for autonomous space RVD between two spacecrafts. The lidar can search and track cooperative targets in a large region without artificial guidance. The lidar's operational range spans from 18 m to 20 km, and the relative angle between two aircrafts can be measured with high accuracy. A novel fiber laser with tunable pulse energy and repetition rate is developed to meet the wide dynamic detection range of the lidar. This paper presents the lidar system's composition, performance, and experimental results in detail.

OCIS codes: (010.3640) Lidar; (140.3510) Lasers, fiber; (120.6085) Space instrumentation; (280.3400) Laser range finder.

http://dx.doi.org/10.1364/AO.54.002470

1. Introduction

Over the past decades, rendezvous and docking sensors (RVD) have been developed, manufactured, and applied successfully in some space missions [1]. An acquisition, pointing, and tracking (APT) lidar can acquire information on the relative angular position, distance, and velocity of a target with high accuracy. The operational ranges of lidars span from several meters to dozens of kilometers. It is a very effective method for autonomous space RVD with cooperative targets. It has been studied for the application of RVD.

The Laser Range Scanner (LARS) developed by the Canadian Space Agency is a versatile 3D sensor for space applications that is capable of performing surface imaging, target ranging, and tracking [2,3]. It is capable of short-range (0.5–20 m) and long-range (20 m–10 km) sensing using time-of-flight (TOF) methods. The LARS was used to obtain target-based measurements, feature-based measurements, and image-based measurements on the STS-52 shuttle flight in October 1992. The Laser Mapper (LAMP), developed by the NASA Jet Propulsion Laboratory [4], is a flight-qualified laser radar that can form 3D images by emitting high-power, short-duration laser pulses and by having a gimbaled mirror. The Spaceborne Scanning Lidar System (SSLS) is a space-qualified scanning lidar system developed by MDA and Optech. The SSLS was integrated onto the XSS-11 spacecraft in 2005, and its maximum operational range is 5 km. The SSLS has already successfully illustrated its ability of long- and medium-range object acquisition and tracking [5]. The Advanced Video Guidance Sensor (AVGS), developed by NASA/MSFC, is a continuation and advancement of the Video Guidance Sensor, which flew successfully on

1559-128X/15/092470-07$15.00/0

Table 1. Specifications of the Lidar

Item	Specification
Transmitter	Pulsed fiber laser Wavelength: 1030 nm Pulse repetition frequency: 5 kHz/50 kHz Average power: 1 nW–1.8 W
Receiver	Telescope diameter: 50 mm FOV: 2.5 deg in full angle Optical filter bandwidth: 3 nm Detector: silicon QAPD
Signal processor	Initial acquisition time: 90 s (limited) Data output rate: 10 Hz Range precision (maximum): 2 m (1–20 km) 0.1 m (18 m–1 km) Line-of-sight angle accuracy: 0.0755 deg (2–20 km) 0.0169 deg (18 m–2 km)
Physical	Mass: <10 kg Power supply: 47.8 W
Cooperative target	Effective reflection area: 50 cm^2

STS-87 and STS-95 [6]. The AVGS was designed to provide a line of sight bearing from greater than 1 km and to provide 6 degrees-of-freedom relative position data from three hundred meters to dock.

Since November 2011, China has successfully completed space RVD between tiangong1 and shenzhou8, 9, and 10 several times [7]. APT lidars were also applied successfully to the RVD missions, which were developed by the 27th Research Institute of China Electronics Technology Group Corporation and the Institute of Optics and Electronics, Chinese Academy of Sciences.

According to the roadmap of the moon explorer in China, the RVD sensor will be implemented between the satellite and the sampling spacecraft. In this paper, a lidar is proposed to search and track cooperative targets from 18 m to 20 km, under a relative attitude angle of ±60 deg in both azimuth and elevation. The relative speed of both spacecrafts is 20 m/s, which corresponds to a line-of-sight angle rate of 2.8 deg/s. The operational ranges of the RVD lidars implemented in past space missions were less than 5 km, which is much less than this system's operational range. The composition, detection mechanism, and experimental results of this lidar will be described in detail in this paper.

2. System and Principle

A. System Design

The maximum range, accuracy of angle, and the initial acquisition time are the most important factors for designing a lidar system. The main specifications of the lidar are listed in Table 1. The architecture diagram of the lidar is shown in Fig. 1. It is composed of a pulsed fiber laser, scanning mechanics, an optoelectronic receiver, a quadrant avalanche photodiode (QAPD), signal processor, and a command controller.

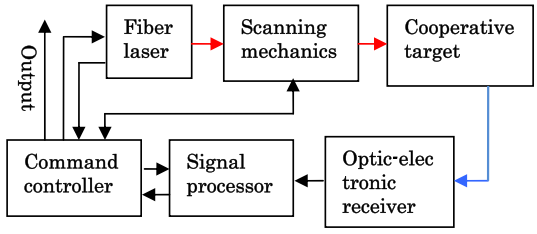

Fig. 1. System architecture diagram of the APT lidar.

The output laser pulses from the pulsed fiber laser at 1030 nm are reflected by a fast steering mirror (FSM) and a two-axis rotating mirror to illuminate a cooperative target. The laser pulse width is 7 ns. The return laser beam is collected by a telescope with a diameter of 50 mm. A solar filter with a bandwidth of 3 nm is inserted before the detector and a silicon-based QAPD (QA4000, First Sensor) with a diameter of 2 mm is used. A digital signal processor (DSP) is developed to retrieve angle and range information. The command controller is also based on DSP to control the scanning system, and to synchronize the laser trigger and signal digitization.

Photographs of the APT lidar system and the cooperative target are shown in Fig. 2. The cooperative target is composed of 34 retroreflectors, and the effective reflection area is 50 cm^2.

B. Method of APT

The whole operating process of the lidar can be divided into three stages as shown in Fig. 3; these are search, acquisition and positioning, and target tracking. The target's highest relative speed and the

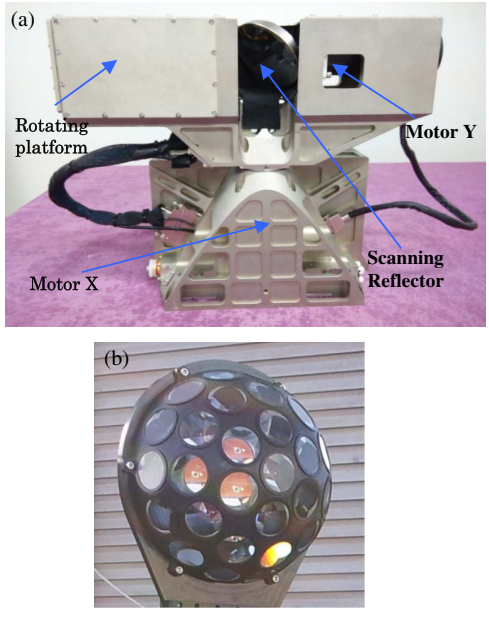

Fig. 2. Photograph of (a) the APT lidar system and (b) the cooperative target.

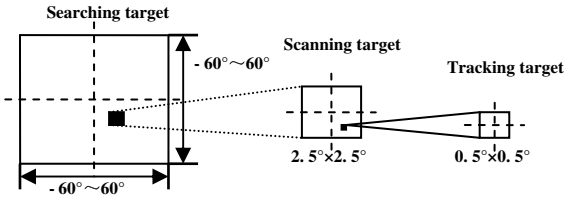

Fig. 3. APT process of the lidar system.

limitation of the initial acquisition time must be considered during all stages.

In the first stage, the surveying angle range of the lidar is 120° × 120°. The laser's divergence angle is set to be 10 mrad and the repetition rate is 50 kHz. In order to ensure no blind area in the search area, the adjacent scanning laser spot has a two-third overlap. Considering the motor's angular position error and the fluctuations of the rotating motor, the motor's scanning step angle is set to 2.6 mrad and the scanning rate in the vertical direction is 21 Hz. Figure 4 shows the scanning routine map. The rotational speed of the motor rotating in the vertical direction (Y) is much greater than the rotational speed of the motor rotating in the horizontal direction (X). If three continuous effective echo signals are detected, the system confirms that the target has actually been acquired. According to the data from the photoelectric shaft encoders of the motors, the angular position is recorded and is calculated approximately. Because the maximum range is 20 km and the laser pulse repetition rate is 50 kHz, the exact rang is hard to retrieve for the reason of an ambiguous range. In order to get a more precise position, the system moves to the next stage.

In the second stage, the FSM of the lidar system is used to scan the target. The scanning field of view (FOV) of the FSM is 2.5° × 2.5° and the scanning rate is 100 Hz. The scanning angle is the same as the FOV of the receiving telescope to maintain the target in the FOV. The laser's repetition frequency is reduced to 5 kHz to overcome the ambiguous range. Different amplitudes of the QAPD are used to calculate an accurate angular position, and the sum signal of four pixels is used to measure the relative range.

In the final stage, the staring FOV of the APT lidar system is 0.5° × 0.5°. The two-axis motors and the FSM are both controlled to stare the target through

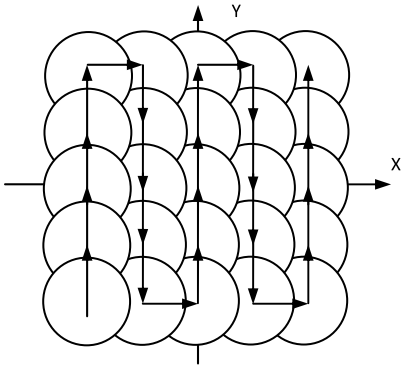

Fig. 4. Rectangle raster scanning way.

analyzing the angle of the lidar-target line of sight in the FOV. The relative angular position, velocity, and distance of the target can be measured more accurately.

C. System Composition

The following sections describe the main units of the lidar such as the laser transmitter, scanning mechanics, optoelectronic receiver, signal processor, and command controller.

1. *Laser Transmitter*

A high-repetition-rate pulsed fiber laser was selected to be the candidate for the transmitter. The pulsed fiber laser is much robust, has high efficiency, and has pulse energy and repetition rate that are easy to change. The pulse fiber laser is configured based on the MOPA (master oscillator power amplifier) structure [8]. The setup and photography of the pulsed fiber laser is shown in Fig. 5.

The laser wavelength is designed to be 1030 nm, because the silicon QAPD's response efficiency is about double that of the conventional wavelength of 1064 nm. According to the operation principle, the laser's energy and repetition can be adjusted according the target's relative range. During the scanning stage, the laser is implemented with a repetition frequency of 50 kHz and maximum energy. After the target is acquired, the laser's repetition rate is changed to be 5 kHz and the laser's energy is divided into 10 levels. The laser energy is switched into different levels according the relative range between two spacecrafts. Figure 6 shows the different energy of each level at 5 and 50 kHz.

2. *Scanning Mechanics*

The scanning unit consists of a two-axis motor scanner and a piezo-based FSM. The servo motors were

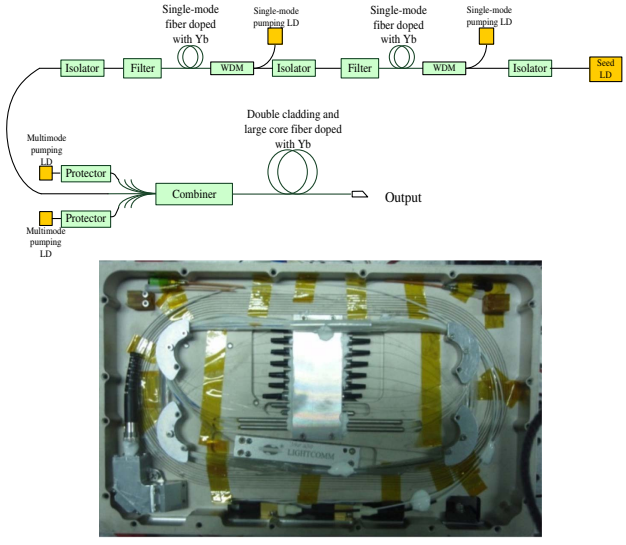

Fig. 5. Setup (top) and photography (bottom) of the all-fiber pulsed amplifier.

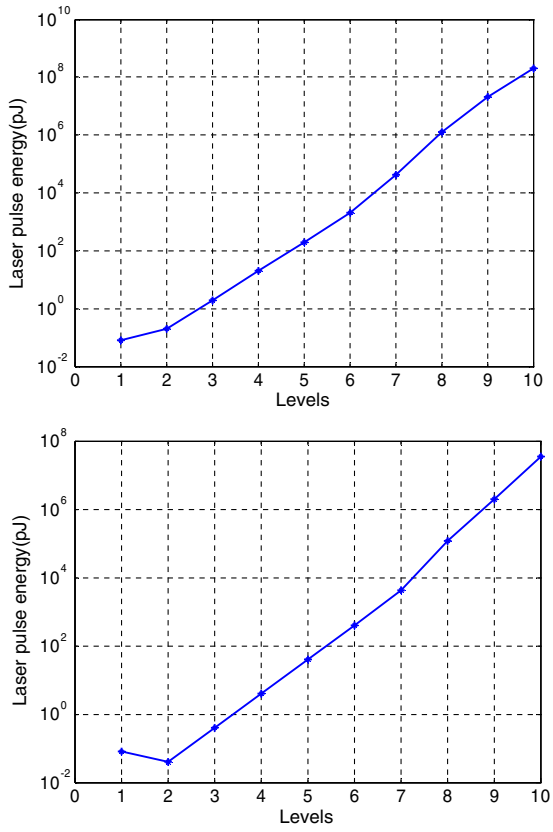

Fig. 6. Output laser pulse energy at different levels: the repetition frequencies are 5 kHz (top) and 50 kHz (bottom).

utilized for scanning on both axes as shown in Fig. 7. The digital controller SJM320F2812 is chosen as the motor drive. Based on the signal received by the QAPD, the position of the target can be calculated. After DSP processing, the control signal of the two-axis motor is calculated. Then the control signal is sent to the motor drive to change the state of the motor. High-precision photoelectric shaft-position encoders are used to feedback the angular position of the motors to the command controller. The angular position precision of the photoelectric shaft-position encoders can reach 0.006°. The auxiliary scanning part is a two-dimensional FSM that is used for scanning rapidly in a small angle range. Its angular position precision can reach 0.05 mrad.

3. *Optoelectronic Receiver*

The receiving optical system is a receiving telescope as shown in Fig. 7, and the receiving FOV is 2.5°. The efficiency of the receive aperture is 50 mm. A QAPD is used as a position-sensitive detector. The detection circuits, shown in Fig. 8, mainly consist of a multistage amplifier circuit and a peak hold circuit. Four same detection circuits are connected to every pixel of the QAPD, and peak hold circuits are connected behind every amplifier. The signal's amplitude used for angular position calculation and for changing the laser pulse energy is transmitted to the signal

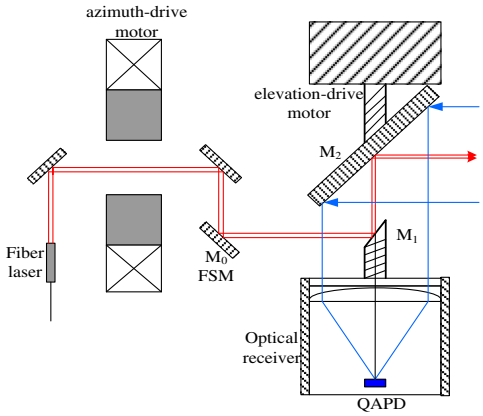

Fig. 7. Scanning mechanics.

processor. The signal after shaping is used as the stop signal for the time detection circuit (TDC).

4. *Signal Processor and Command Controller*

As shown in Fig. 9, this module is mainly responsible for signal processing, controlling the whole system, information acquisition, and transmission.

The signal processor is used for angular position and distance measurement. Distance can be acquired with the TDC, which is achieved with a field programmable gate array (FPGA) chip and a TDC-GPX chip. The target distance can be measured by measuring the TOF of the laser pulse [9], and the time measurement precision of the TDC is 81 ps. The angular position is calculated with the signal amplitude in different quadrants of the QAPD [10].

A DSP chip is used to control the whole system. It collects information from the fiber laser, signal processor, the photoelectric shaft-position encoders of the motors, and the temperature sensor. The DSP sets up the pump laser diode's (LD's) current parameters of the fiber laser to change the output laser pulse energy according to the signal amplitude of the QAPD. If the signal reaches saturation, the pump LD's current is cut down. According to the information from the photoelectric shaft-position encoders and the signal-processing module, the angular position can be calculated accurately. At the same time, the two-axis motor scanner and the piezo-based FSM are both con-

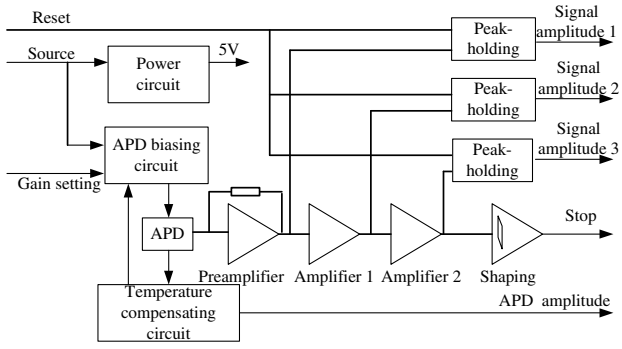

Fig. 8. Amplifier and peak hold circuit for one pixel of the QAPD.

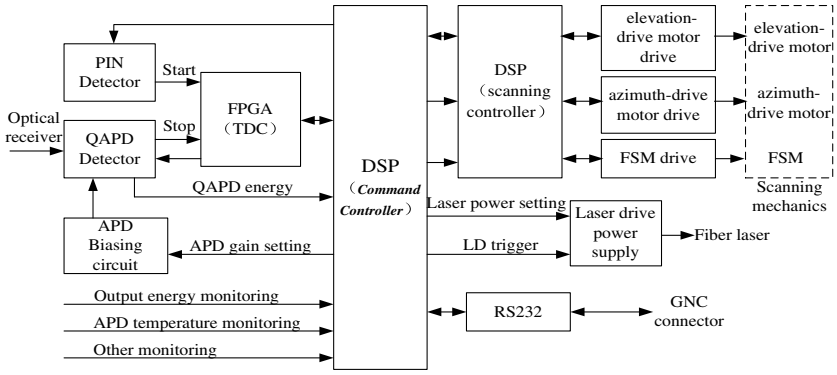

Fig. 9. System architecture diagram.

trolled to stare the target through analyzing the angle of the lidar-target line of sight in the FOV.

3. Experiment Results and Discussion

In this section, the basic functions and specifications of the lidar are discussed. The initial acquisition time, maximum operational range, and the precision of the angle and range are examined. Three test scenarios are implemented, including a simulation platform, an *in situ* experiment with short distance, and an *in situ* experiment between two mountains.

A. Initial Acquisition Time and Maximum Detectable Range

The lidar system is installed on a high-precision two-dimensional rotating platform. The angular precision of the rotating platform in the horizontal direction is 0.0045° and that in the vertical direction is 0.0049°.

The rotation speed can be set to be similar to the relative speed between two spacecrafts. The experimental scene is shown in Fig. 10. In this experiment, the cooperative target is located in a building downtown at a distance of about 1 km. When the platform is rotating, the lidar system can search and track the cooperative target automatically. The acquisition time is less than 90 s at a relative line-of-sight angle rate of 2.8 deg/s.

With the same experimental platform, the maximum range is checked. The cooperative target is still located at 1 km. According to the actual laser energy

Fig. 10. Lidar mounted on a two-dimensional rotating platform.

and the atmospheric visibility (D), the maximum operational range can be calculated by changing the transmitter laser energy, if the illuminating laser spot is large enough compared with the cooperative target at the test range. The difference between the test range and the maximum operational range is merely the different transmitted energy and atmospheric attenuation.

In order to estimate the atmospheric attenuation coefficient, a visibility meter is installed in the building during the experiments. The atmospheric attenuation coefficient σ can be calculated according to visibility D [11] as follows:

$$\sigma = \frac{3.91}{D}\left(\frac{\lambda}{0.55}\right)^{-q}; \tag{1}$$

$$q = \begin{cases} 1.6, & \text{good visibility} \\ 1.3, & \text{moderate visibility} \\ 0.585D^{1/3}, & D \le 6 \text{ km} \end{cases}.$$

Therefore, the maximum range can be described as follows:

$$R_{\max} = \left(\frac{E_{\text{trans}}}{E_{\text{exp}}} \cdot \frac{1}{\exp(-2\sigma R_{\text{test}})}\right)^{1/4} \cdot R_{\text{test}}, \tag{2}$$

where E_{trans} and E_{exp} are the maximum laser pulse energy and the energy at the experimental distance, respectively. R_{test} is the range measured in the experiment.

The transmitted laser energy is attenuated step by step, and the lidar system should keep tracking the target with enough accuracy. During the experiment, the atmospheric visibility D is 4 km. When the laser energy is attenuated to be 400 pJ, the lidar system still tracks the target. According to the design of the system, laser energy of 34 μJ will be used at the maximum range. Therefore, the maximum range can be calculated as follows:

$$R_{\max} = \left(\frac{34\ \mu\text{J}}{400\ \text{pJ}} \cdot \frac{1}{\exp(-2\sigma R_{\text{test}})}\right) \cdot R_{\text{test}}, \tag{3}$$

where R_{test} is about 1 km; therefore, the maximum operational range is about 24.3 km. The result agrees well with that predicted by the system.

In order to verify the actual maximum range, the test is conducted between two mountains at a distance of 18.95 km in Kunming, Yunnan province of China. During the experiment, the atmospheric visibility is about 20 km. The lidar system still worked well to search and track the target.

B. Range Precision

Range precision is tested at different ranges. The lidar system is still installed on the two-dimensional rotating platform as shown Fig. 7. The target is located at a distance of 20.8 m. The lidar system keeps tracking the target, and 50 measurements are recorded. Thus, the range precision can be calculated as follows:

$$3\sigma = \sqrt{\frac{\sum_{i=1}^{50}[d_i - d_s]^2}{49}} \times 3, \tag{4}$$

where d_s is the practical distance and d_i is the distance measured. The measurement is shown in Fig. 11, and the range precision (3σ) around 20.8 m is 0.096 m. Here, 3σ is regarded as the system's measurement precision, and the probability of the actual measurement precision exceeding 3σ is very little. This will ensure the reliability of the system.

The range precision at medium and long ranges is also evaluated. Figure 12 shows the distances measured at 4252.7 m and 18.95 km. The range precisions (3σ) are 1.24 and 1.56 m at distances of 4252.7 m and 18.95 km, respectively.

C. Angular Precision

Similarly to the range precision testing scene, angular precision is demonstrated. The lidar system is fixed on the two-dimensional rotating platform. The rotating platform is turned by α_s in the horizontal direction, and the system provides the angular data α_a and α_b at the starting and ending points, respectively. This yields 50 continuous angle data. Taking the average of the angle values at the starting point

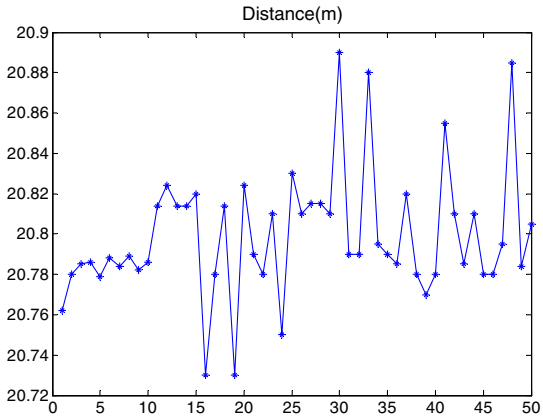

Fig. 11. Range testing at 20.8 m.

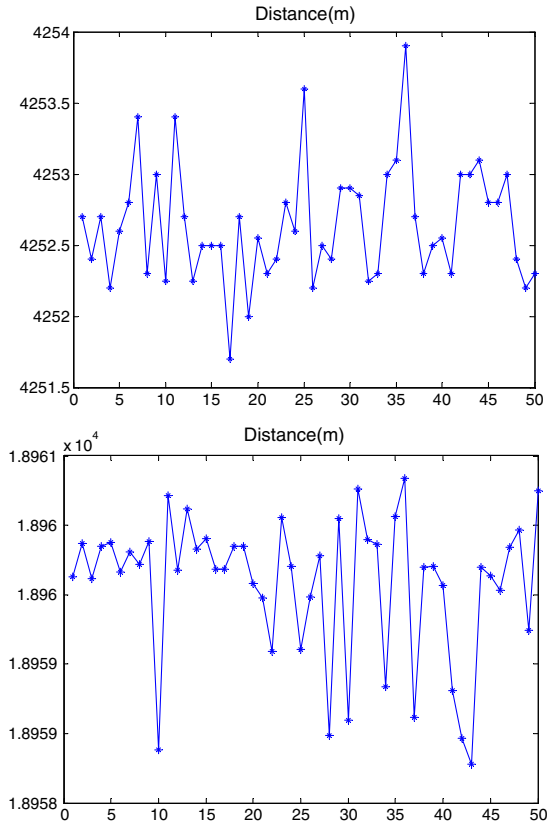

Fig. 12. Range test at 4252.7 m (top) and 18.95 km (bottom).

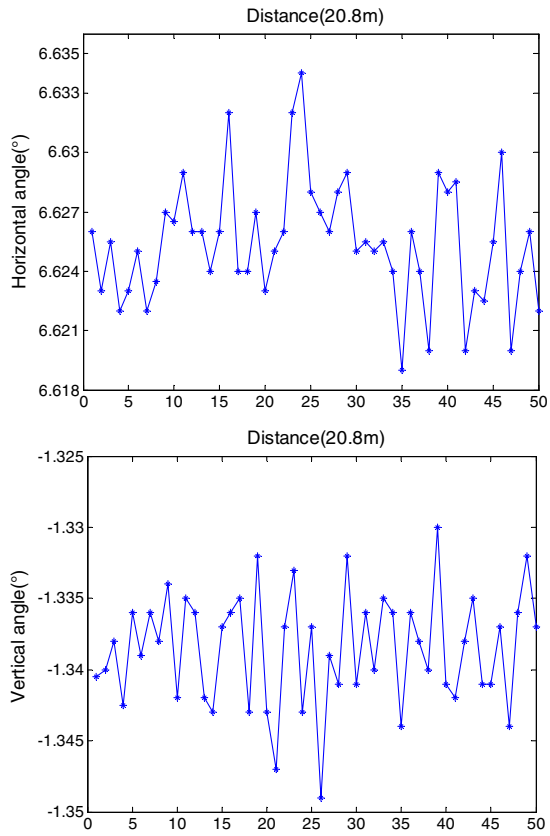

Fig. 13. Angle data in the horizontal direction (top) and vertical direction (bottom).

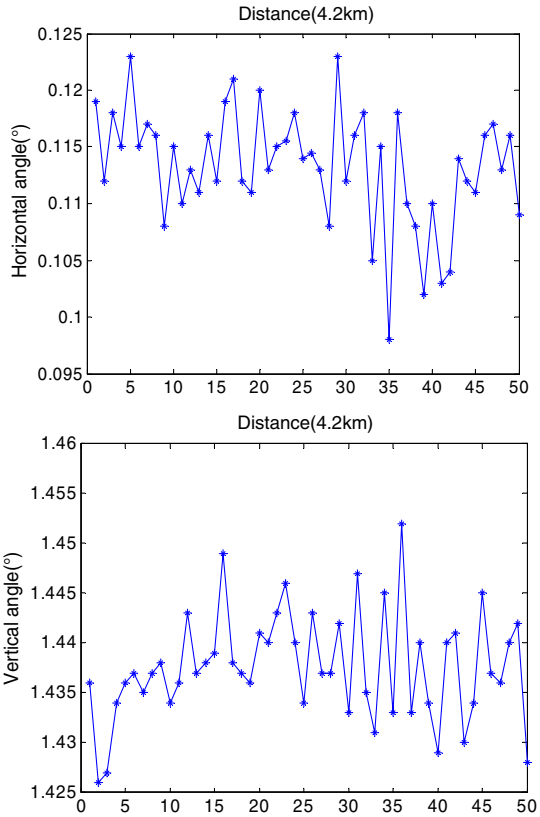

Fig. 14. Angle data in the horizontal direction (top) and vertical direction (bottom).

and evaluating the angular precision, the evaluation formula is

$$3\sigma_\alpha = \sqrt{\frac{\sum_{i=1}^{50}[|\alpha_{bi} - \overline{\alpha_a}| - \alpha_s]^2}{49}} \times 3. \quad (5)$$

Then the rotating platform is turned by β_s in the pitching direction, and the system yields the angular data β_a and β_b at the starting and ending points, respectively. This yields 50 continuous angle data. Taking the average of the angle data at the starting point and evaluating the angular precision, the evaluation formula is

$$3\sigma_\beta = \sqrt{\frac{\sum_{i=1}^{50}[|\beta_{bi} - \overline{\beta_a}| - \beta_s]^2}{49}} \times 3. \quad (6)$$

When the target is at 20.8 m, $\alpha_s = 5.719°$, $\alpha_a = 0.906°$, $\beta_s = 2.192°$, and $\beta_a = 0.853°$. The 50 continuous angular data are shown in Fig. 13. According to formulas (5) and (6), the angular precision in the horizontal direction is 0.0093°, while the angular precision in the vertical direction is 0.012°.

When the target is at 4.2 km, $\alpha_s = 5.719°$, $\alpha_a = 5.606°$, $\beta_s = 2.192°$, and $\beta_a = -0.754°$. The 50 continuous angular data are shown in Fig. 14. According to formulas (5) and (6), the angular precision in the horizontal direction is 0.016°, while the angular precision in the vertical direction is 0.016°.

4. Conclusions

The APT lidar technology is one of the key technologies used in space RVD. This paper presents a new type of APT lidar based on a high-repetition-frequency pulsed fiber laser. The effective range of the lidar can span from 18 m–20 km. It can well achieve the functions of searching and tracking a cooperative target in a predictable region without artificial guidance. The fiber laser used in the lidar system has played a very important role in reducing the system's power consumption, volume, and mass, and has protected the detector and enlarged the operational range of the lidar system. The lidar system's composition, working process, and experimental results have been introduced in detail in this paper. Through a large number of experimental verifications, the lidar system has perfectly achieved the functions of acquisition, pointing, and tracking, and all indices (angular precision, range precision, power consumption, volume, and mass) satisfy the needs of practical application.

References

1. B. Moebius, M. Pfennigbauer, and J. Pereira do Carmo, "Imaging lidar technology-development of a 3D-lidar elegant breadboard for rendezvous and docking, test results, and prospect to future sensor application," in *International Conference on Space Optics* (Rhodes, 2010), pp. 4–8.
2. J. A. Beraldin, F. Blais, M. Rioux, L. Cournoyer, D. G. Laurin, and S. G. MacLean, "Short and medium range 3D sensing for space applications," Proc. SPIE **3074**, 29–46 (1997).
3. D. Laurin, J.-A. Beraldin, F. Blais, M. Rioux, and L. Cournoyer, "A three-dimensional tracking and imaging laser scanner for space operations," Proc. SPIE **3707**, 278–289 (1999).
4. C. C. Liebe, A. Abramovici, R. K. Bartman, R. L. Bunker, and J. Chapsky, "Laser radar for spacecraft guidance applications," in *IEEE Aerospace Conference*, 2003, Vol. **6**, pp. 2647–2662.
5. M. Nimelman, J. Tripp, G. Bailak, and J. Bolger, "Spaceborne scanning lidar system (SSLS)," Proc. SPIE **5798**, 73–82 (2005).
6. S. Van Winkle, "Advanced Video Guidance Sensor (AVGS) project summary," Proc. SPIE **5418**, 10–20 (2004).
7. Y. C. Xie, H. Zhang, J. Hu, and H. Hu, "Automatic control system design of Shenzhou spacecraft for rendezvous and docking," Sci Sin Technol. **44**, 12–19 (2014).
8. Y. J. Chiang, C. S. Hsiao, and L. K. Wang, "Optimization of erbium-doped fiber MOPA laser," Opt. Commun. **283**, 1055–1058 (2010).
9. S. M. Nejad and S. Olyaee, "Comparison of TOF, FMCW and phase-shift laser range-finding methods by simulation and measurement," Q. J. Technol. Educ. **1**, 11–18 (2006).
10. M. Toyoda, K. Araki, and Y. Suzuki, "Measurement of the characteristics of a quadrant avalanche photodiode and its application to a laser tracking system," Opt. Eng. **41**, 145–149 (2002).
11. H.-X. Wang and A. Ye, "The influence of the coefficient of atmospheric attenuation to the capability of laser ranging," Ship Sci. Technol. **29**, 116–119 (2007).